J. Phys. A: Math. Gen. **30** (1997) 3421–3440. Printed in the UK PII: S0305-4470(97)77496-1

Symbolic dynamics for hydrogen in a magnetic field

Kai T Hansen† and Stefan Güttler‡

Fakultät für Physik, Universität Freiburg, Hermann-Herder-Strasse 3, D-79104 Freiburg, Germany

Received 27 August 1996, in final form 11 March 1997

Abstract. We discuss symbolic dynamics for the Hamiltonian describing the classical motion of hydrogen in a uniform magnetic field with zero angular momentum. For a scaled energy above a critical value ϵ_c, the Hamiltonian has a Cantor set repellor described by a three-lettered symbolic alphabet. For energies below ϵ_c it is not proven that a good symbolic dynamics description exists. We propose and investigate several methods to determine a symbolic dynamics, and conjecture that these methods label uniquely all non-escaping trajectories for $\epsilon \geqslant 0$ and most trajectories for $\epsilon < 0$. We define well ordered symbols and construct the pruning front which determines the admissible orbits, the information needed for effective semiclassical resonance spectra computations.

1. Introduction

The problem of describing a charged particle moving in an attracting Coulomb field combined with a constant magnetic field has a long history, it has been reviewed by Friedrich and Wintgen [1], Hasegawa *et al* [2] and Delande [3]. In this article we introduce and apply a symbolic description for this class of smooth Hamiltonian flows. We believe that the methods we develop are well suited to analyse a number of physically interesting Hamiltonian systems. In semiclassical calculations for chaotic systems, symbolic dynamics is essential in order to have a description of all periodic orbits [4, 5]. In a previous article, semiclassical quantization of hydrogen in a magnetic field has been carried out for scaled energies larger than a critical value for which the repellor is a complete Cantor set [6]. In order to extend these semiclassical calculations to lower scaled energy ranges, one needs an effective symbolic dynamics description of the non-complete Cantor set structure of the orbits. We describe here the first step in this direction while the actual semiclassical calculation is left as future work.

Symbolic dynamics is the representation of a trajectory as a string of symbols, and in a number of hyperbolic systems it has turned out to be a fruitful way of investigating the classical flow in phase space. It was used by Smale in his description of the simplest chaotic dynamical system, the horseshoe map [7]. Our problem is, for some parameter values, a map similar to a Smale horseshoe map; this fact will be a very useful starting point for our investigation. The other important class of systems where symbolic dynamics can be rigorously defined are billiards [8]. One billiard of special interest for the problem at hand

† Present address: NORDITA, Blegdamsvej 17, DK-2100 Copenhagen Ø, Denmark. Also at: Physics Department, University of Oslo, Box 1048, Blindern, N-0316 Oslo, Norway. E-mail address: khansen@nordita.dk

‡ Present address: Max-Planck-Institut für Physik komplexer Systeme, Bayreuther Strasse 40, 01187 Dresden, Germany. E-mail address: guettler@idefix.mpipks-dresden.mpg.de

0305-4470/97/103421+20$19.50 © 1997 IOP Publishing Ltd

is the n-disk scattering system [9, 10]. The symbolic dynamics for n-disk systems can be used as a 'covering' dynamics also in the cases where the set of admissible orbits is not a complete Cantor set. For billiard systems one can prove the existence of an infinite but countable Markov partition [8]. In this article we will extend the method developed for pruned billiards and apply it to smooth Hamiltonian flows.

We will describe three ways to define symbols for a smooth flow. They are different ways to view the same problem, with different advantages and disadvantages, but none of them can avoid the rather complicated structure discussed below. As we shall show, the trajectories which give the border between allowed and forbidden orbits form a fractal set in phase space, so the definition of symbolic dynamics has to be rather complicated.

One elementary method is to look in configuration space for trajectories having special properties to be specified below. The second method counts caustics along a trajectory in configuration space and determines the border where one caustic vanishes. The third method finds stable-/unstable-manifold tangency points, which yield a partition curve in the Poincaré plane. This method also reveals interesting details of structures characteristic in smooth systems in general, such as the 'avoided crossings'. The last two methods can be used to calculate the 'pruning front', needed for approximate Markov partitions. Combining the three different methods provides a powerful approach to a detailed understanding of the classical dynamics of the system.

Bifurcations of classical periodic orbits in hydrogen in a magnetic field have been described in a number of articles, for example [1, 11], but not systematically using symbolic dynamics as is done here. We restrict ourself to the system where the angular momentum parallel to the magnetic field is zero. The azimuthal quantum number is then zero in the quantum mechanical system [1]. If there is a non-zero angular momentum the centripetal force yields a very different dynamics.

In section 2 we review the symbolic dynamics of the four-disk billiard. In section 3 we discuss the definition of symbols in configuration space and how the stability matrix can be used to associate symbols to smooth Hamiltonian flows. Section 4 describes the construction of a partition curve in the Poincaré plane. In section 5 the concept of pruning fronts is introduced and section 6 describes a simple application of the theory; a calculation of the topological entropy using dynamical zeta functions. Section 7 gives the conclusions.

2. Symbolic dynamics of four-disk billiards

To simplify the understanding of the structure of the trajectories for the hydrogen atom in a magnetic field we start by reviewing the symbolic dynamics and the structure of manifolds for a four-disk system. Figure 1(a) shows the bounded billiard system bordered by four touching disks in the two-dimensional configuration space and the path of a point particle bouncing elastically off the borders along a periodic orbit. The symmetric four-disk system in figure 1(a) has a C_{4v} symmetry and can be tiled using $\frac{1}{8}$ of the original configuration space [27]. We call this small configuration space the fundamental domain of the system, figure 1(b). We now describe different methods of assigning a symbol sequence to a given trajectory.

A disk is placed in each of the four quadrants of the configuration plane and the canonical symbolic dynamics is given by the string $S = \ldots s_{-1}s_0s_1s_2\ldots$, where s_t is the label of the disk where the point particle collides at bounce number t. For example, the symbol string of the periodic orbit in figure 1(a) is $(1234)^\infty \equiv \overline{1234}$. If four disks are sufficiently separated by any infinitely long string (with the exception of strings with $s_t = s_{t+1}$) it corresponds to a possible path for the point particle. In this case there exists a complete Cantor set repellor

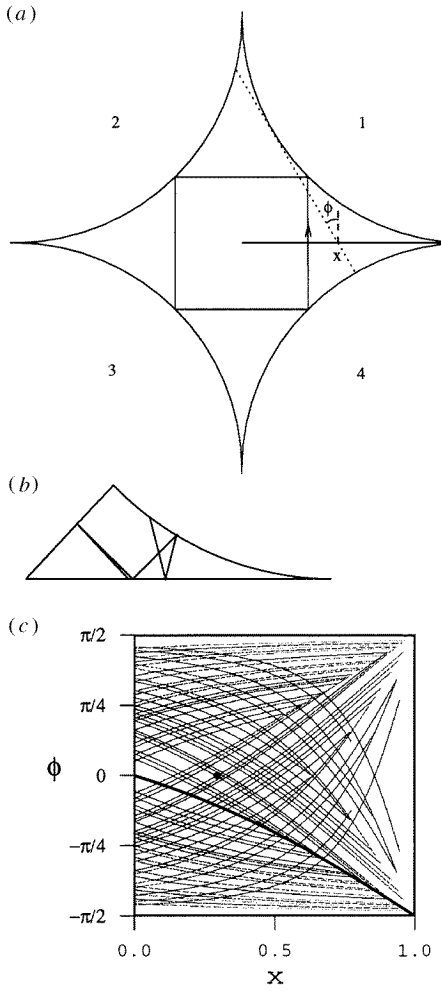

Figure 1. (*a*) The touching four-disk billiard and the periodic orbit $S = \overline{1234}$. (*b*) The fundamental domain of the four-disk billiard. (*c*) The manifold structure for the periodic orbit $\overline{1234}$ (marked with with a •), and the partition line for the touching four-disk billiard.

equivalent to a Smale horseshoe map with three folds. If the disks are close together such as in figure 1(*a*) some of the symbol strings are inadmissible, and the corresponding orbits have disappeared through inverse bifurcations as the disks move closer to each other [17]. This system is an example of a *pruned* horseshoe map.

The pruned horseshoe map is drawn in figure 1(*c*), using a part of the unstable and stable manifolds of the periodic orbit $\overline{1234}$ in figure 1(*a*). The Poincaré section (x, ϕ) chosen here is the crossing of a trajectory with one of the coordinate axis, with x denoting the distance from the origin and ϕ denoting the angle anticlockwise from the normal vector, see figure 1(*a*). An equivalent choice for the second coordinate is to use p_x which is proportional to $\sin\phi$. In addition to the stable and unstable manifolds we have drawn the *partition curve* (heavy line) which corresponds to paths which start at (x, ϕ) and then touch disk number 1 tangentially; an example is drawn with a dotted line in figure 1(*a*). The partition curve in the Poincaré plane yields an alternative way to define the same symbolic dynamics as introduced above. A point in the Poincaré section above the partition curve corresponds to a trajectory bouncing off a disk before the next crossing of the Poincaré section, while a point below the partition curve yields a trajectory that does not bounce.

The corresponding symbol is determined by the quadrants of the configuration space in which the bounce takes place.

A third way to define the same symbols is to follow two very close parallel neighbour trajectories through a quadrant and check whether the trajectories cross each other. If the trajectories bounce off a disk, then they will cross each other. If the trajectories do not cross we do not get any symbol, but if they cross we give a symbol to the trajectories according to the label of the quadrant in which the crossing took place. For billiards this yields a symbolic description identical to the above two methods, and the procedure can to some degree be used in smooth potentials where the concept of a 'bounce' is not as clear as it is for billiards.

The inadmissible orbits are simplest to describe in a well ordered symbol plane [15, 12–14]. This symbol plane (γ, δ) is defined from our disk enumerating symbols by using the algorithm [12]:

$$\begin{aligned} &v_t = s_t - s_{t-1} \\ &\text{if } v_t < 1 \qquad \text{then } v_t = v_t + 4 \\ &w_t = \begin{cases} v_t - 1 & \text{if } t \text{ odd} \\ 3 - v_t & \text{if } t \text{ even} \end{cases} \\ &\gamma = 0.w_1 w_2 w_3 \ldots = \textstyle\sum_{t=1}^{\infty} w_t/3^t \\ &\delta = 0.w_0 w_{-1} w_{-2} \ldots = \textstyle\sum_{t=1}^{\infty} w_{1-t}/3^t. \end{aligned} \tag{1}$$

Mapping the partition curve of figure 1(*c*) into this symbol plane yields the *pruning front*, the border of the region with symbol strings corresponding to forbidden orbits in the system.

3. Symbolic dynamics for the smooth system

We will now generalize the symbolic dynamics of hyperbolic billiards described in the previous section to a smooth Hamiltonian flow, hydrogen in a uniform magnetic field.

3.1. Hydrogen in a uniform magnetic field

The non-relativistic Hamiltonian for the hydrogen atom in a homogeneous magnetic field $\boldsymbol{B}$ along the z-axis is given as

$$H = \frac{p^2}{2m_e} - \frac{e^2}{r} + \frac{1}{2}m_e\omega^2(x^2 + y^2) + \omega L_z. \tag{2}$$

The z component of the angular momentum L_z is conserved, and we shall consider only the $L_z = 0$ case here. The reduced mass is denoted by m_e, and the frequency $\omega = eB/2m_e c$ is half the cyclotron frequency. Rewritten in cylindrical coordinates and atomic units the Hamiltonian (2) is given by

$$H = E = \frac{p_z^2}{2} + \frac{p_\rho^2}{2} - \frac{1}{\sqrt{\rho^2 + z^2}} + \frac{1}{8}\gamma^2\rho^2 \tag{3}$$

where $\gamma = B/B_0$ is the magnetic field strength written in units of $B_0 = m_e^2 e^3 c/\hbar$, and ρ is the radial distance from the z-axis. The system is bounded for $E < 0$, while for $E > 0$ almost all trajectories escape to $z = \pm\infty$ with non-zero kinetic energy.

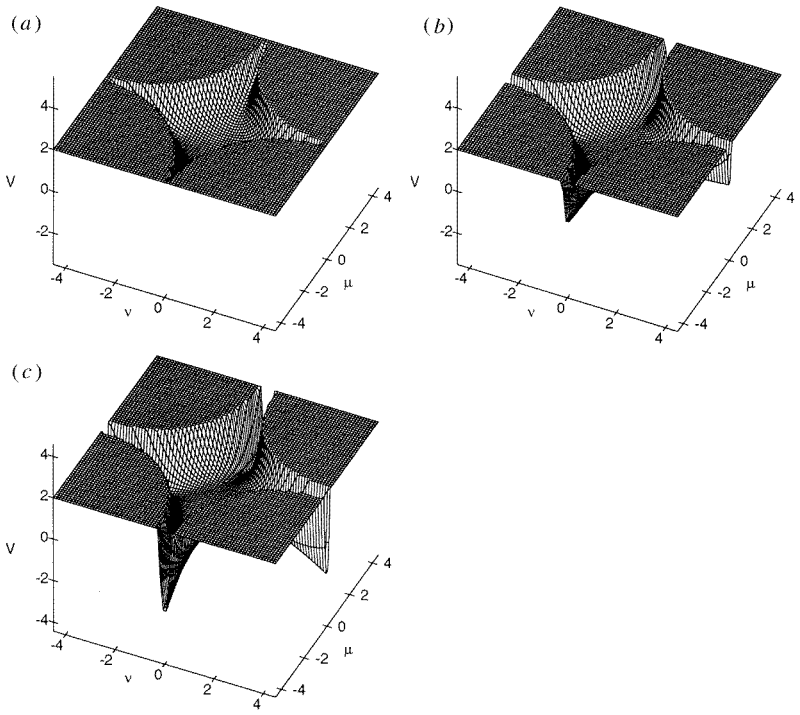

Figure 2. The potential of (4) for (*a*) $\epsilon = -0.1$, (*b*) $\epsilon = 0$, and (*c*) $\epsilon = 0.1$.

As described in [1], it is convenient to introduce a scaled energy $\epsilon = \gamma^{-2/3}E$. The Hamiltonian (3) written in semi-parabolic coordinates (ν, μ) can then be transformed into

$$h = \tfrac{1}{2}p_\nu^2 + \tfrac{1}{2}p_\mu^2 - \epsilon(\nu^2 + \mu^2) + \tfrac{1}{8}\nu^2\mu^2(\nu^2 + \mu^2) \equiv 2. \tag{4}$$

h is parametrized only by the scaled energy ϵ and equals the fixed pseudoenergy 2. In the remainder of this paper we will work with the Hamiltonian (4) only.

The potential in (4) is drawn in figure 2 for a few different values of ϵ. The potential is cut off when it exceeds the value of 2.0 since the Hamiltonian (4) is always identical to the value of 2. For $\epsilon > 0$ the potential looks like a smooth analogue to the open four-disk billiard with four hills giving rise to reflections and four valleys along which the electron can escape. For $\epsilon < 0$ the electron cannot escape and the potential resembles a bounded four-disk billiard. The potential also has the C_{4v} symmetry like the four-disk billiard, and we define a fundamental domain in the same way as for the disk system, choosing the octant $\nu > 0$, $\mu > 0$, and $\mu < \nu$. The (ν, μ) plane is divided into four quadrants by the coordinate axes, and labelled anticlockwise as for the four-disk billiard.

We choose as our Poincaré section (x, p_x) in the fundamental domain the crossing of the trajectory with either one of the axes ν or μ. The value of x is the position $|\nu|$ or $|\mu|$ and p_x is the momentum component parallel to the axis, positive in the direction away from the origin.

3.2. Coding

A natural way to define symbolic dynamics in the smooth system is to code the trajectories as we did in the four-disk billiard. This was first suggested by Eckhardt and Wintgen [16]

and is motivated by the similarity of the equipotential lines for hydrogen in a magnetic field for $\epsilon \geqslant 0$ with a hyperbola- or four-disk billiard. Bifurcations in a closed billiard where the walls are chosen to be exactly the equipotential lines ($\epsilon < 0$) are discussed in [19].

Eckhardt and Wintgen [16] proposed a symbolic description for unstable periodic orbits for $\epsilon \geqslant 0$ using the stability matrix. Their method is analogous to the method of determining symbols in the disk system, where we check if neighbouring trajectories cross in a quadrant of the configuration space. This defines a 'bounce' in the smooth system. The definition is more complicated in a smooth system than in billiards because the crossing points may move outside the quadrant and will depend on where we choose to start looking at a trajectory. Eckhardt and Wintgen [16] restricted their discussion to unstable periodic orbits and by using self-focal points which are specific to unstable periodic orbits, they obtained a definition of symbolic dynamics for the orbits they tested. We will discuss and apply here a generalization of this method to non-periodic trajectories.

In the four-disk system we found a simple partition curve in the Poincaré plane and used this to define the symbolic dynamics. We propose here to determine such a curve also for the smooth system. The advantage of this method is that it is fast, accurate and simple to use, while the disadvantage is that the determination of this curve in a smooth system is a non-trivial task. A partition curve of this type was first proposed by Grassberger and Kantz [20] for the Hénon map. Defining symbolic dynamics using a partition curve has been discussed for different systems in [15, 14, 21].

3.3. Manifold structure

Figure 3 shows the unstable periodic orbit in the smooth potential analogous to the $S = \overline{1234}$ orbit in the four-disk system. Figure 4 shows a part of the unstable and stable manifolds for this orbit plotted in the Poincaré plane for $\epsilon = 0.35$, $\epsilon = 0.0$, and $\epsilon = -0.1$. In figure 4(a) we have also drawn a proposed partition curve; the line $p_x = -x$ is analogous to the partition curve in the four-disk system. We are free to choose any curve we like in a band around this line. The band is bounded by the closest crossing points between the stable and unstable manifolds in figure 4(a).

In figure 5 we have drawn five trajectories ($\epsilon = 0.35$) in the configuration space. Two trajectories (dotted curves) are starting from points below the partition curve in figure 4(a), two from points above the partition curve (broken curves), and one exactly on the partition curve (full curve). In the first quadrant the broken curves have a bend, a 'bounce' marked on the figure, while the dotted curves do not bend in this way at all. We therefore give the symbol 1 to the broken curves in this first quadrant while the broken curves are not given any symbol in this quadrant. The trajectory drawn with a full line in figure 5 starts at the partition curve and escapes from the system, while bouncing back and forth between quadrants 1 and 2. In figure 4(a) we find that for $\epsilon = 0.35$ there are no tangencies between stable and unstable manifolds. Our definition of symbolic dynamics using the partition line in figure 4(a) then gives a unique labelling of all trajectories which do not escape from the system, neither in the past nor the future. Points on the partition line escape directly either forwards or backwards (or both) in time. This system is a type of Smale horseshoe repellor with the special property of stretching out to $x = \infty$. At the point $x = \infty$ the manifolds do not cross each other at a finite angle and the system is not hyperbolic at this point. This property gives rise to the intermittency discussed in [6]. This is the structure for the system for all $\epsilon > \epsilon_c = 0.328\ldots$ [22].

Escaping trajectories cannot be uniquely encoded but are also not interesting in most applications. A systematic search for escaping trajectories must, however, use symbolic

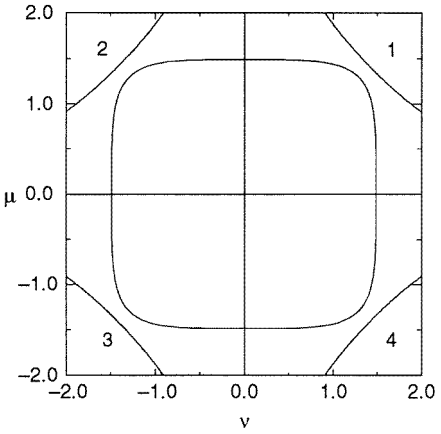

Figure 3. The periodic orbit $S = \overline{1234}$ for $\epsilon = 0$.

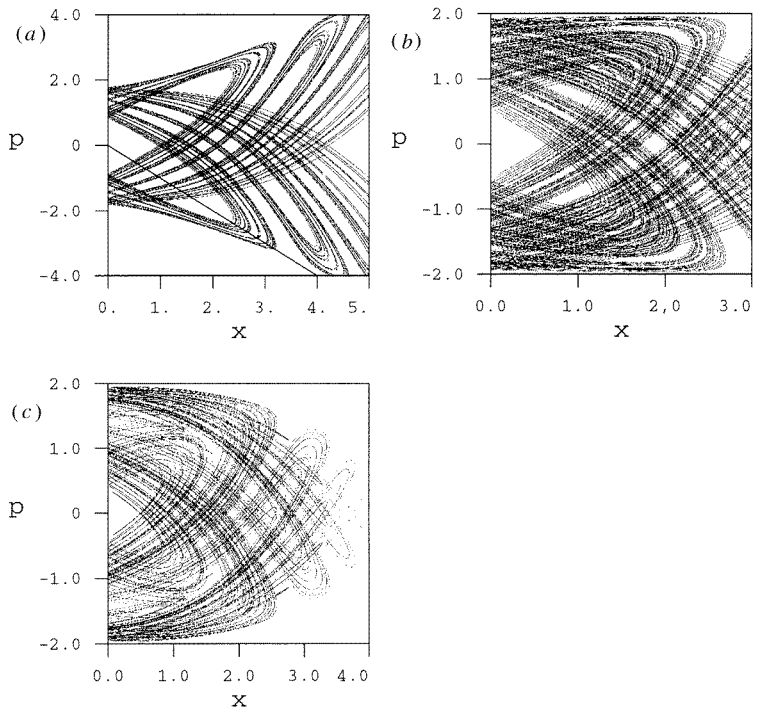

Figure 4. A part of the stable and unstable manifolds of the periodic orbit in figure 3. (*a*) $\epsilon = 0.35$, (*b*) $\epsilon = 0.0$, and (*c*) $\epsilon = -0.1$. In (*a*) a partition curve is drawn.

dynamics to find the areas of starting points that give the families of similar escaping orbits.

It is not obvious that a similar partition can be made for other parameter values such as in figure 4(*b*) or (*c*), where *homoclinic tangencies* exist, i.e. points where the stable and unstable manifolds are tangent to each other. Systems with homoclinic tangencies are not complete horseshoe repellors and may in general contain islands of stability. We nevertheless conjecture that it is possible to define a partition curve in the Poincaré plane

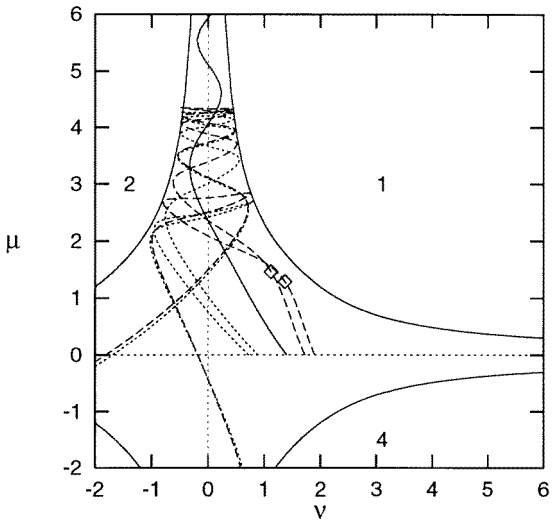

Figure 5. Five trajectories for $\epsilon = 0.35$. One starting at the partition line in figure 4(a) and escaping, two starting above the partition line bouncing (broken curves), and two starting below the partition line with no bounce in the first quadrant (dotted curves).

for $0 \leqslant \epsilon < \epsilon_c$. We believe that the partition curve is also well defined for $\epsilon < 0$, but in that case additional bifurcation structures have to be considered.

3.4. Extremal trajectories

One way of determining a partition between trajectories with different symbolic dynamics is to use trajectories which are *extremal* in configuration space. For $\epsilon > \epsilon_c$ we can determine for each fold of the unstable manifold the orbit which escapes fastest towards ∞. This orbit attains an extremum position in configuration space. It is further away from the origin than its neighbour trajectories at a given time, and it yields a partition point on the fold of the unstable manifold. This means, that on one chosen fold of the unstable manifold there will be a pair of two starting points, one on each side of the partition point, which converge towards each other in the future. Since they are points on the same fold, they converge towards each other also in the past. These two trajectories must have different symbolic codes in order to get a unique symbolic dynamics description, and this is obtained by choosing different symbols according to whether the trajectory starts on the right or the left side of the extremum orbit in this quadrant.

The set of trajectories from all starting points on a fold of the unstable manifold is a bundle of trajectories starting on both sides of the extremal orbit in configuration space but ending up on only one side of the extremal trajectory. This is illustrated in figure 5 for a large energy, and in figure 6 for a smaller energy. Determining all extremal trajectories yields a symbolic dynamics description for all non-escaping trajectories which is identical to the partition curve in figure 4(a) for $\epsilon > \epsilon_c$.

Also for $\epsilon < \epsilon_c$ we have extremal trajectories in the configuration space, defined such that trajectories starting on different sides of the extremal trajectory end up on the same side in configuration space after some time (and the same for negative time). Figure 6 shows this for $\epsilon = 0$ for an extremal trajectory and two neighbour trajectories on each side. At each bounce the ordering of neighbouring trajectories flips and the extremal trajectory is extremal in the 'opposite way' in the configuration plane after a bounce. A special case occurs when the extremal trajectory, after a number of bounces, coincides with another extremal trajectory. We discuss this case below as it turns out to give 'gaps' in the partition

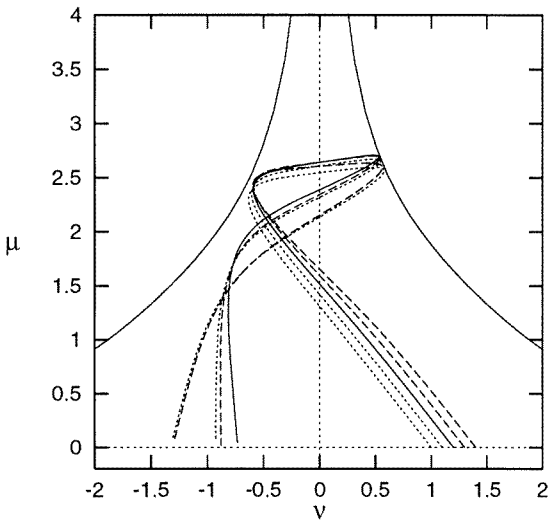

Figure 6. Five trajectories for $\epsilon = 0.0$ showing that there is an extremum path in the configuration space.

line. Since all extremal trajectories escape directly for $\epsilon > \epsilon_c$, in this case there will not be any trajectory which is extremal twice and consequently there are no gaps. However, determining extremal trajectories from looking at orbits in the configuration space is not a practical method. A closely related method using the stability matrix is preferable.

3.5. The stability matrix

A *caustic* is an envelope of the turning points of trajectories coming from a point, see [4], and we identify a caustic with what we call a bounce in the smooth flow. Caustics are closely related to conjugate points [4] which can be determined from the *stability matrix*. The stability matrix is a 4×4 matrix describing the linearized motion along a trajectory in phase space. As discussed by Eckhardt and Wintgen [23], this 4×4 matrix can be reduced in a local coordinate system to a 2×2 matrix

$$\mathbf{M} = \begin{pmatrix} M_{11} & M_{12} \\ M_{21} & M_{22} \end{pmatrix}. \tag{5}$$

The eigenvalues of $\mathbf{M}$ yield the stability coefficients of the trajectory.

A caustic occurs in configuration space when the value of M_{12} is equal to 0. This may seem simple to calculate but there are some difficulties in using this method. The set $\{M_{12} = 0\}$ yields points, which are conjugate to the starting point of the trajectory, where $\mathbf{M}(t = 0) = I$. These points depend therefore on the starting point and are not fixed along a given trajectory. However, the dependence on the initial condition becomes very small as one follows the trajectory for a long time. We can therefore locate quite well the conjugate points $M_{12} = 0$ along a long trajectory and assign a symbol to each conjugate point. In most cases, we obtain a good symbolic description using this method.

An example is given in figure 7 where the conjugate points along a trajectory are marked with black dots, yielding the symbolic dynamics string for this trajectory $S = \ldots 12141414134213232343343 \ldots$. The symbols are chosen as for the four-disk billiard. If the trajectory bends sharply then there is a $M_{12} = 0$ dot indicating a bounce at the bending

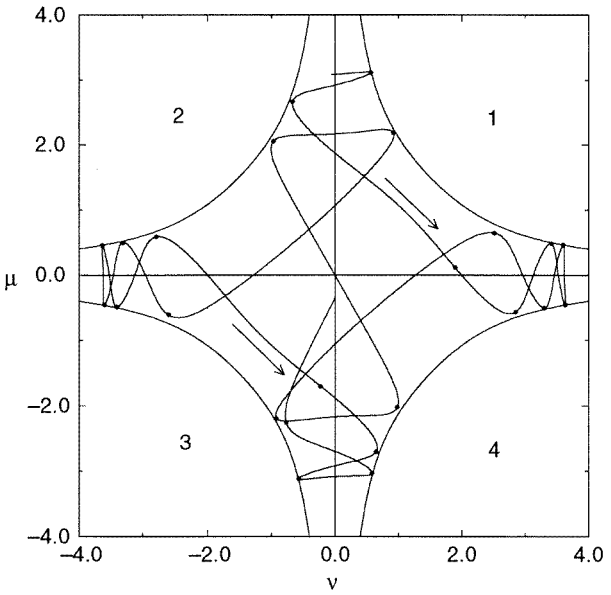

Figure 7. A trajectory in configuration space with dots indicating where the element M_{12} of the stability matrix is 0 ($\epsilon = 0.2$).

point. But when the bounce is weak the conjugate point tends to get pushed forward along the trajectory to a position after the maximum bending point. This behaviour is typical and leads to the difficulties of this method.

The difficulty is illustrated in figure 8(a). This trajectory has a bounce in the first quadrant, but the corresponding zero of M_{12} gets smoothly pushed forward along the trajectory into the adjacent quadrants as we approach the border from 'bouncing' to 'not bouncing' in the first quadrant. In figures 8(b)–(d) we choose starting points closer and closer to the transition from 'bouncing' to 'not bouncing' in the first quadrant. Here the $M_{12} = 0$ point corresponding to the first bounce is seen to move forward along the trajectory, as indicated with an arrow. In order to obtain a good symbolic description using the zeros of M_{12}, we have to check if two consecutive dots appear in the same quadrant. If this occurs, we let one of these zeros indicate the symbol of a weak bounce in a previous quadrant. Because tracing back a zero of M_{12} along the trajectory may be ambiguous, errors in the symbolic code may arise. In practical applications however, it turns out, that only a small number of trajectories are affected by the assignment of a possibly ambiguous symbolic code.

The property of a conjugate point to get pushed forward along the trajectory is related to the behaviour of the additional crossing point between the broken trajectories in comparison with the dotted trajectories in figure 6. Here we also find that if we choose starting points closer to the extremal trajectory, the additional crossing point moves forward to an adjacent quadrant. The proper extremal trajectory is therefore only defined in the limit $t \to \pm\infty$.

The detection of extremal trajectories, i.e. the determination of starting points of trajectories where the total number of zeros of M_{12} changes by one, can in most cases be done with good accuracy using the stability matrix method.

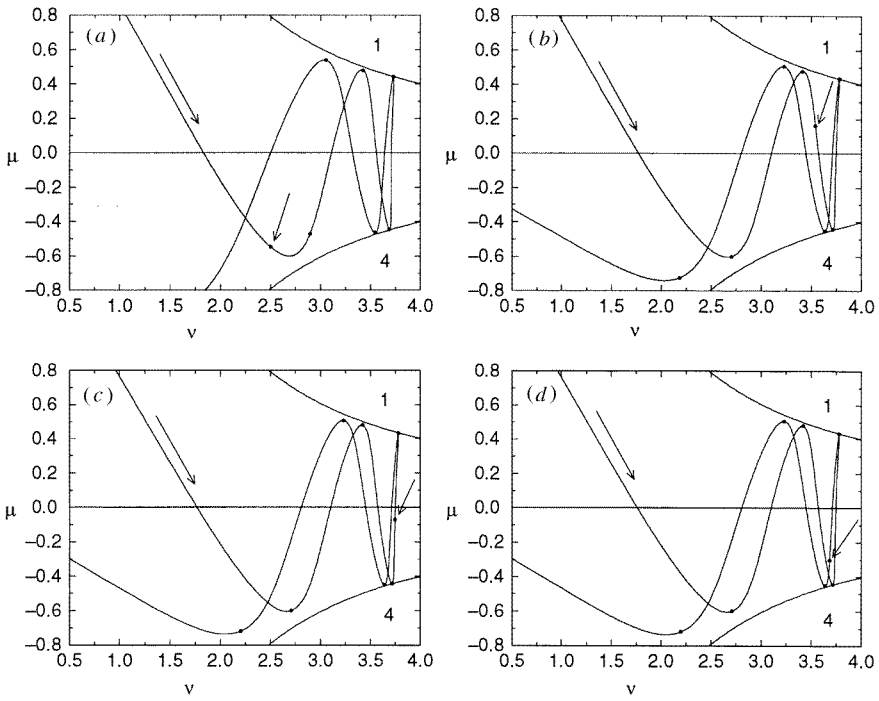

Figure 8. Trajectories with $M_{12} = 0$ dots as the trajectory approaches an extremal trajectory. $p_x = -p_y$, $\epsilon = 0.2$, (*a*) $x = y = 0.930$, (*b*) $x = y = 0.886$, (*c*) $x = y = 0.882$, (*d*) $x = y = 0.880\,54$.

4. The partition curve in the Poincaré plane

4.1. Primary turning points

As we discussed above, orbits that are extremal in configuration space give a partition between bouncing and not bouncing trajectories. The images of these orbits in the Poincaré plane are either tangent points between the stable and the unstable manifolds (a homoclinic or heteroclinic tangency) or points not belonging to both the unstable and the stable manifold. We denote these the *turning points* of the manifold. There are two problems in using these turning points to define a partition curve in the Poincaré plane. One problem is that each turning point has an infinite number of images and preimages. For a closed system this set of images and preimages of all turning points is dense in phase space, and also for open systems this set is large and complicated. Only one image from each turning point can be used in the partition curve. A second problem is that the set of turning points is usually not a simple smooth curve but a disconnected fractal set. A partition line should be continuous and therefore contain sections that connect the turning points.

The first problem requires choosing one among all images of a turning point that we want to use as a point on the partition line. We call the chosen point the *primary turning point*. In maps such as the Hénon map [20] or the standard map [21] there is no obvious way to choose which turning point should be called primary. A generic scheme has been proposed for maps of the Hénon-type in [14].

For the hydrogen in a magnetic field we have the advantage, that each turning point

is associated with a trajectory in configuration space. This trajectory is bordering between 'bouncing' and 'not bouncing' in some quadrant. We call this the *critical* bounce of the trajectory. The intersection of this trajectory with the Poincaré plane right before the trajectory enters the quadrant where it has its critical bounce, yields the primary turning point. The trajectory is called singular in this quadrant. All other intersections of the singular trajectory with the Poincaré plane (earlier or later) yield non-primary turning points. This gives some restrictions on the choice of the primary turning points. It turns out, that singular trajectories coincide (as expected) with trajectories, which are extremal in configuration space.

Numerically we can find turning points using a method introduced in [24]. This method determines the points on the unstable manifold where the curvature of the manifold diverges under iterations forward in time. This method is much faster and simpler than looking at pictures of manifolds and determining the tangency point from pictures. Since this system is intermittent, the manifold from one periodic orbit penetrates very slowly into some areas of the Poincaré plane. We may therefore need to iterate other segments of unstable manifolds to cover the regions of interest.

Figure 9 shows the primary turning points determined by this method for the $\epsilon = 0$ case of figure 4(b). We have also included points of symmetry curves as discussed below.

4.2. Gaps between primary turning points

The turning points shown in figure 9 have the structure of 'avoided crossings'. An avoided crossing appears when the trajectory belonging to a primary turning point crosses the Poincaré plane close to another primary turning point. In a hyperbolic billiard with non-smooth manifolds we have a simple crossing of the smooth partition curve with a non-smooth image of this curve, as illustrated in figure 10(a), where the dotted curves indicate turning point curves. For a smooth potential the manifolds are smooth, and we get, instead, a structure where the curve through primary turning points is connected to a curve through non-primary turning points. This breaks the crossings in the disk system figure 10(a) into

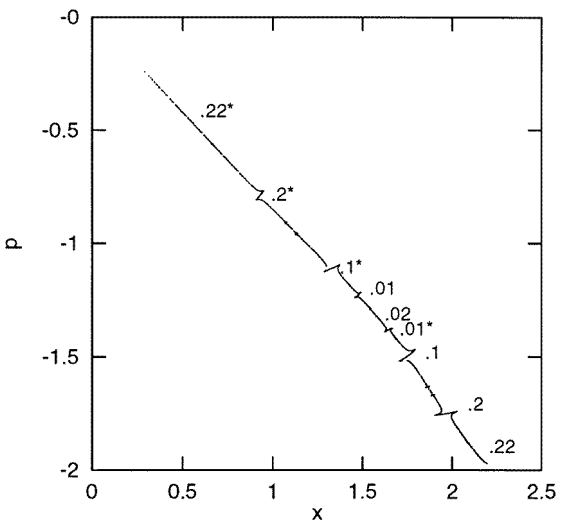

Figure 9. The partition curve for $\epsilon = 0$, compare with figure 4(b).

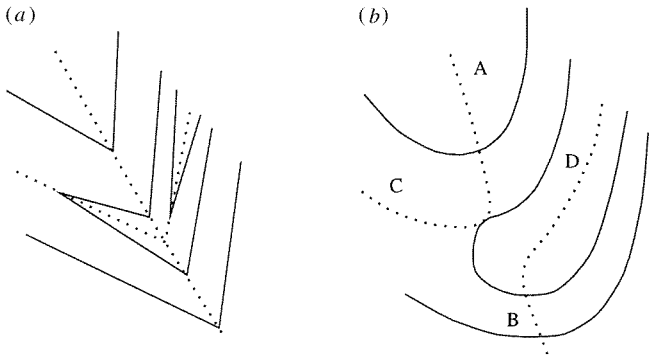

Figure 10. A sketch of the manifold structure close to (*a*) a crossing for a hyperbolic billiard, (*b*) an avoided crossing for a smooth system.

an avoided crossing structure for the smooth system as sketched in figure 10(*b*).

We find that trajectories bouncing critical in the first quadrant and having a weak bounce after n bounces (primary turning points giving curve A in figure 10(*b*)) merge together with those trajectories having a weak bounce in the first quadrant and then a critical bounce after n bounces (non-primary turning points giving curve C in figure 10(*b*)). Similarly, we have a merging of trajectories which first have a critical bounce and then are close to, but do not bounce after n bounces (primary turning points giving curve B in figure 10(*b*)) those trajectories which in the first quadrant do not bounce but then have a critical bounce after n bounces (non-primary turning points giving curve D in figure 10(*b*)).

We know the trajectory between two critical bounces and can label the corresponding gap using the symbolic dynamics of the trajectory. We label it by the well ordered symbols, because we then get an indication of the relative position of the gap in the Poincaré plane. There are 2×3^n possible gaps created from trajectories bouncing $(n + 1)$ times between the two critical bounces. For a given parameter value ϵ only a subset of these 2×3^n gaps will be present. The factor of 2 appears because one cannot have a bounce in the quadrant opposite to the quadrant with a critical bounce and that leaves us with just two choices of a next bounce. From this argument it follows that the last critical symbol in the well ordered symbol string, as defined in (1), is a critical $w_n = 0$ or a critical $w_n = 2$ symbol. All other bounces are non-critical bounces in one of the three remaining quadrants giving the factor of 3^n. To obtain a simple ordered number for the gap, we have to rename the last symbol $w_n = 1$ if it was a critical $w_n = 0$ and keep the last symbol $w_n = 2$ if it was a critical $w_n = 2$. We then get γ_g analogous to (1) from the finite sum

$$\gamma_g = \sum_{t=1}^{n} w_t/3^t. \tag{6}$$

Each trajectory between two critical bounces yields four gaps in the Poincaré plane. One gap is obtained in the Poincaré plane where a trajectory enters the first quadrant having a critical bounce (I), and a second gap appears when this trajectory enters another quadrant with a second critical bounce (II). The same trajectory followed in the time-reversed direction also gives two gaps; one when entering the second quadrant (III) and one more when entering the first quadrant (IV). These four points are indicated in figures 11(*b*) and (*d*).

However, if one orbit turns back and retraces itself, the gaps (I), (III) and (II), (IV) are identical, and in this case we only get two gaps. The trajectory in figure 11(*b*) is symmetric

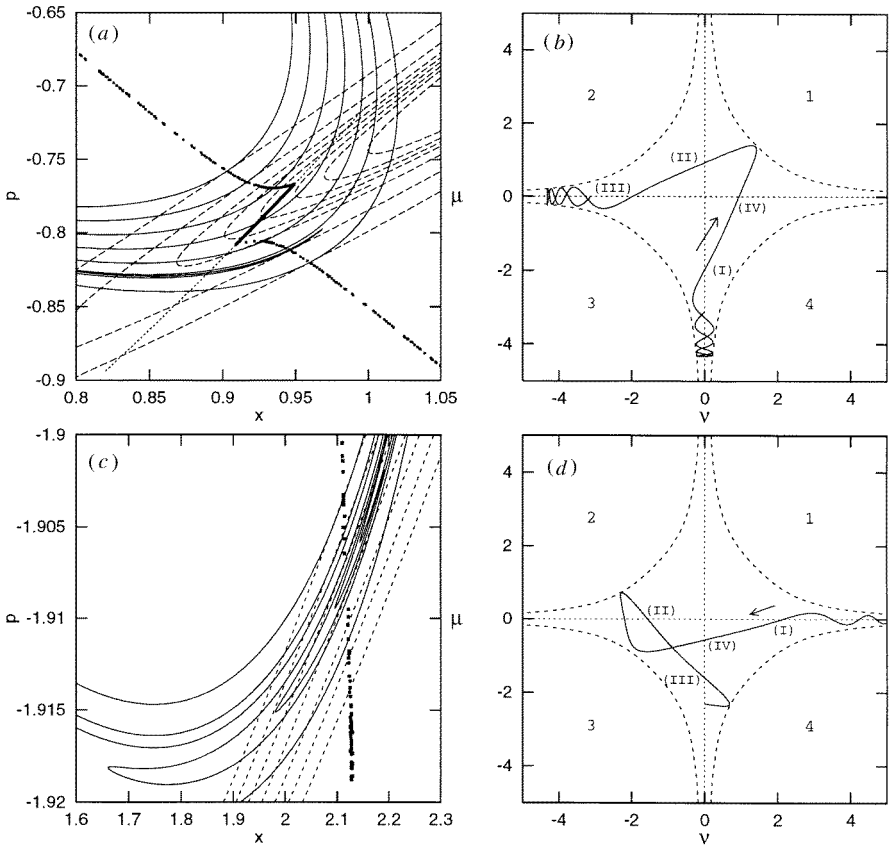

Figure 11. Gaps in the turning point curve and the trajectory close to this gap. (*a*) The gap and (*b*) the corresponding symmetric trajectory $\gamma_g = 0.1$. (*c*) The gap and (*d*) the corresponding non-symmetric trajectory $\gamma_g = 0.22$.

in the full (μ, ν) space and self-retracing in the fundamental domain. Since we are using a Poincaré map of the fundamental domain, it is sufficient that orbits retrace themselves there. Trajectories with a spatial symmetry in the full configuration space will be self-retracing in the fundamental domain and therefore yield only two gaps.

The well ordered symbols we use to label the gaps are a symbolic dynamics description in the fundamental domain, so we get two labels for the trajectories which are not self-retracing and one for the self-retracing trajectories. We then finally get two gaps for each γ_g. One of these gaps is ordered according to the value of γ_g while the other gap is not. The latter one would be well ordered if we had labelled gaps by a δ value, equation (1), instead of γ. We indicate γ_g with an asterisk (*) when it describes the gap not following the γ_g ordering.

Not all gaps exist for a given parameter value ϵ, since some gaps are not yet created. This means, trajectories with the symbolic dynamics given by γ_g escape instead of having another critical bounce. For $\epsilon > \epsilon_c$ this is true for all gaps. For $\epsilon < \epsilon_c$ other gaps do not exist because the trajectory between two critical bounces is pruned. In figure 9 we have drawn the primary turning points for $\epsilon = 0$, the gaps are labelled with γ_g and γ_g*.

The size of the gaps depends on the instability of the trajectory between two critical

bounces. We expect that in most cases the size decreases exponentially with the number, n, of bounces between two critical bounces. Only gaps with small n will therefore be important in numerical calculations. This may not be true for intermittent trajectories and trajectories close to stable orbits.

4.3. Construction of a partition curve in the gaps

Because we need a continuous partition curve in the Poincaré plane, we have to bridge the avoided crossings with some curve. For the standard map Christiansen and Politi [21] have argued that one has a large freedom in choosing this bridge, but the largest gaps could be filled by curves obtained by using some symmetry. One special point in the avoided crossing structure is the tangent point Q where the unstable and stable manifolds have the same curvature. At any other tangent point two homoclinic points merge together, but Q is the point where three homoclinic points merge together. This is sketched in figures 12(a) and (b). In figure 12(a) there are four homoclinic tangent points between the unstable manifold (full curve) and the uppermost of the stable manifold (broken line). If we decrease the scaled energy ϵ, the three upper-leftmost homoclinic points move together and bifurcate into one homoclinic point at Q, figure 12(b). At this point there are two homoclinic tangencies which merge together. Instead of changing the energy ϵ, we can instead look at different folds of the unstable manifold. Inside a fold looking like that in figure 12(a) there will be a fold like in figure 12(b) with a bifurcation point Q. This point Q always exists for a bounded system and a corresponding point can be found for the escaping system.

The gaps in the partition curve which correspond to self-retracing trajectories can be bridged by using the spatial symmetry of these trajectories. We choose the curve in the Poincaré section given by the one parameter set of symmetric trajectories to which the orbits having singular bounces belong. These self-retracing trajectories can easily be found numerically and give a smooth curve in the Poincaré plane through Q and a point on the other side of the gap. We conjecture, that using these curves for both the gaps, γ_g and γ_g*, yields a unique coding. In figure 11(a) we have drawn the avoided crossing for the $\gamma_g = 0.1$ gap together with the symmetry line (dotted line). These symmetries exist in the fundamental domain and will be generic for many systems.

The other gaps can be bridged using a piece of the stable or the unstable manifold from Q to the other turning point curve. This has to be done consistently for all four images of the avoided crossing. For the parameter values we have investigated, the largest gaps have retracing symmetry and can be bridged with the symmetry curve. The other gaps are small. If one investigates the very small gaps given by trajectories bouncing a large number of times between the critical bounces, very few of these have retracing symmetry. Figure 11(d)

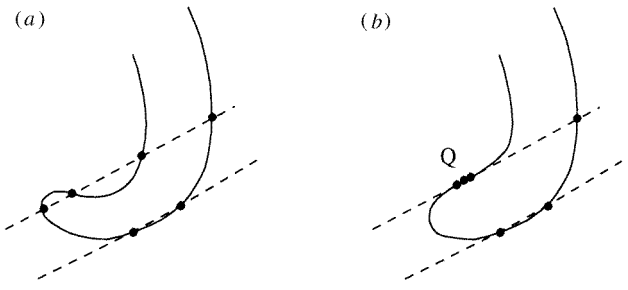

Figure 12. Sketch of the bifurcation point Q where three homoclinic points merge together.

shows a short trajectory without retracing symmetry, $\gamma_g = 0.22$, and the corresponding gap in the Poincaré plane is drawn in figure 11(c). The rather small non-symmetric gaps we found here could be bridged with straight lines in the calculations below.

4.4. Stable islands

A periodic orbit may become stable if the trajectory is close to a singular trajectory. This is the only way one can obtain stable orbits for $\epsilon \geqslant 0$. This implies that in the Poincaré plane stable islands are on or close to the partition curve. Whether we can continue the partition curve through all the islands is an open question, and if this cannot be done we will have to find the symbolic dynamics description of the orbits within each island by some other method. We may find these orbits for a larger ϵ where they are unstable and have a well defined symbolic description and then follow the orbits adiabatically as ϵ decreases. If there is no bifurcation of these orbits with codimensions higher than 1 along this parameter path (that is, the periodic orbit is not close to a Q point), then we can assume that the orbit does not change its symbolic description [25, 14]. For the standard map Christiansen and Politi [21] proposed to use a symmetry line as a partition for some stable islands. It is possible that some islands for hydrogen in magnetic field also have this property.

The symbolic description of the different periodic and non-periodic orbits in an island is the same as the symbolic description of the family of orbits bifurcating together at a singular bifurcation in the four-disk billiard. This is discussed in some detail in [17]. An example of a stable island for $\epsilon > 0$ is given in [22].

5. Pruning

We now turn to the question of admissibility of orbits.

In dispersing billiard systems we obtain a pruning front by mapping the singular tangent trajectories onto the symbol plane (γ, δ). We can map singular trajectories of the smooth system onto the symbol plane in the same way. The set of primary turning points gives our singular trajectories, and we iterate the trajectories forwards and backwards in time and determine their symbolic dynamics by using the partition curve. This yields the picture in figure 13 for $\epsilon = 0$. The area limited by the pruning front is called the primary pruned region.

A quick numerical test of the pruning front is obtained by iterating a large number of initial conditions and plotting the symbolic values of their iterates in the symbol plane. In figure 14 we have drawn these points as black dots; the forbidden (white) areas in this plane appear similar to the results for four-disk billiards and hyperbola billiard [12]. The primary pruned region in figure 13 together with its symmetric images and the forward and backward iterates yield the complete pruning region identical to the white areas in figure 14.

The primary pruned region changes with the scaled energy ϵ. At the critical energy $\epsilon_c = 0.328\ldots$ the pruned region vanishes; it increases as ϵ decreases from this value. In figure 15 we have drawn the pruning fronts for different values of ϵ. The primary pruned region is found here to increase monotonically with decreasing ϵ. It seems numerically to be true that the pruning front always increases for $\epsilon \geqslant 0$, but it is hard to prove rigorously that orbits are only created as ϵ increases and never as ϵ decreases. For $\epsilon < 0$ there are few examples of orbits being created as ϵ decreases [11]. However, we expect this to be a rare occurrence as long as the bifurcations follow qualitatively the bifurcation pattern given by the symmetric four-disk billiards, where the orbits are created monotonically as the distance between disks is increased. For $\epsilon < 0$ also another mechanism causes bifurcations for

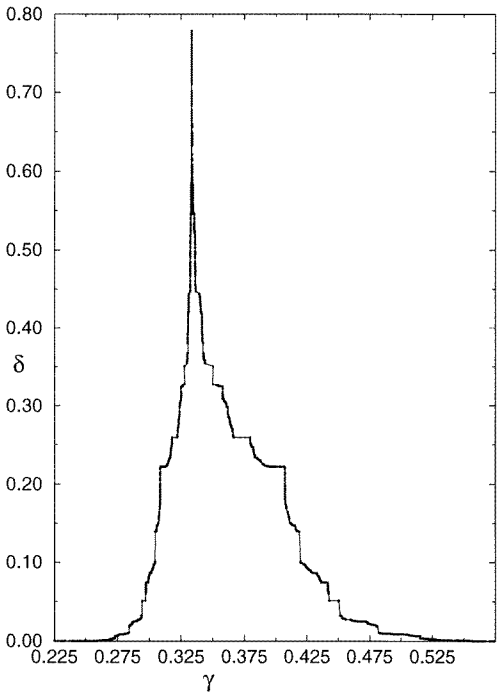

Figure 13. The pruning front in the symbolic plane for $\epsilon = 0$. The points on the pruning front are connected with straight lines to guide the eye.

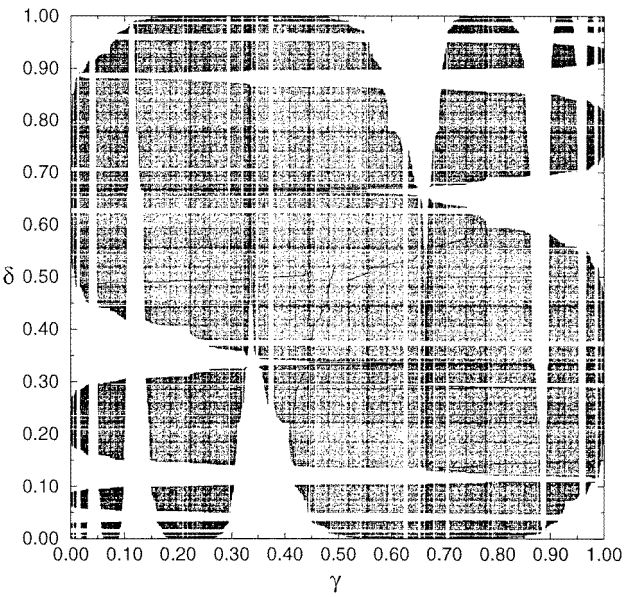

Figure 14. A number of chaotic trajectories plotted on the symbolic plane for $\epsilon = 0$.

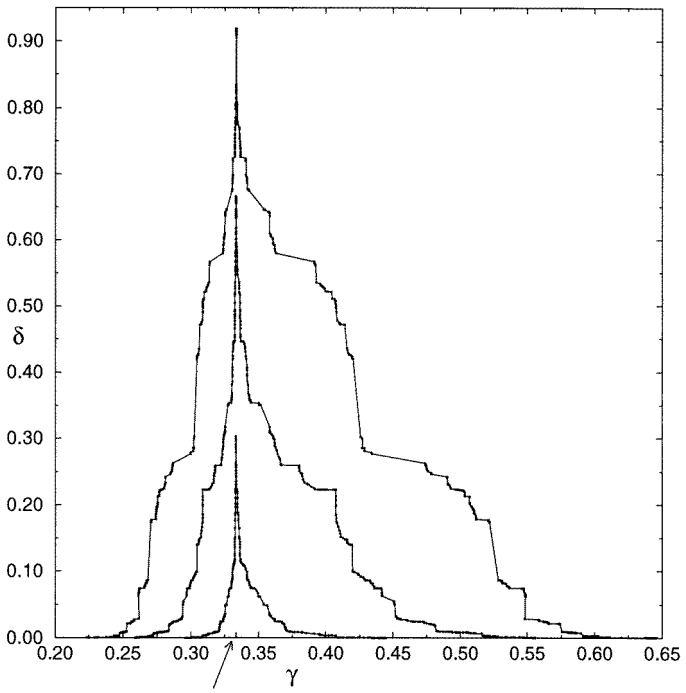

Figure 15. The pruning front for $\epsilon = -0.1$, $\epsilon = 0$, $\epsilon = 0.1$, and $\epsilon = 0.2$ (indicated with the arrow).

hydrogen in a magnetic field. Most of these are related to the bifurcations one has in corner pruning for the four-disk system [14] and will be treated somewhere else.

The pruning fronts in figure 15 were obtained by using the stability matrix method. Here we give symbols to trajectories by using the stability matrix and determine in a binary search the set of orbits whose symbol strings take a maximum value of γ, equation (1). It turns out, that these trajectories become extremal in configuration space and therefore correspond to points on the pruning front in the symbol plane. The comparison of the pruning front for $\epsilon = 0$ in figure 15 with figure 13 shows, that both methods of determining a symbolic dynamics for hydrogen in a magnetic field agree with only small numerical deviations.

6. Applications

One main aim of this work is to provide a systematic approach for determining the periodic orbits necessary for the semiclassical calculation of the resonance spectrum for hydrogen in a magnetic field. This was done in [6] for a simpler case with $\epsilon > \epsilon_c$. In semiclassical calculations there are several other problems, for example that some families of orbits are not truly hyperbolic and we therefore have to redefine the expansion of the zeta function [18, 6]. A proper semiclassical calculation is outside the scope of this article. However, as a first demonstration of a zeta-function calculation, we determine the topological entropy of this system.

6.1. The topological zeta functions

The topological entropy h is the rate of exponential growth of the number of periodic orbits as a function of their length (here we measure length in the number of symbols an orbit is given). The topological entropy can be determined by using the simplest case of a zeta function, where the stability of the orbits does not enter [18]. The zeta function for a system described by a suitable symbolic dynamics can be partitioned into a fundamental term and a curvature term [18]. In the case of the topological zeta function the curvature term cancels completely and only the fundamental term is left giving a 'topological polynomial' (the characteristic polynomial of the Markov graph), if the symbolic dynamics is specified by a finite Markov graph. The topological entropy is given by the leading zero of the topological polynomial. We construct approximate Markov graphs [26, 14] and calculate the topological entropy as we exclude more and more forbidden orbits from our description. The set of all forbidden orbits up to a finite length can be read off from the primary pruned region in the symbol plane [12], see figures 13 and 15.

Figure 16 shows the topological entropy for the approximate Markov graphs as a function of the number of forbidden symbol strings in the trinary alphabet. The convergence is slow because there is a large number of forbidden strings with the same symbol length. For $\epsilon = 0.0$ the longest forbidden string used here has eight symbols, and for $\epsilon = 0.1$ the longest forbidden string used has nine symbols. We find that the topological entropy approaches $h = \log 2.99$ for $\epsilon = 0.1$ and $h = \log 2.90$ for $\epsilon = 0$. From this we can conclude that pruning is not very strong, since $h = \log 3$ for the unpruned case $\epsilon > \epsilon_c$.

7. Conclusions

We have developed and compared several methods of determining the symbolic dynamics for the hydrogen atom in a magnetic field. The method of constructing a partition curve from turning points of the unstable manifold defines symbolic dynamics and describes in detail the very complicated structure of the dynamics. It shows that the trajectories which are bordering between different symbolic descriptions are a fractal set in the phase space. No method of determining symbolic dynamics can avoid this intricate structure, and none describes it as explicitly as the turning point method does. The turning point method also

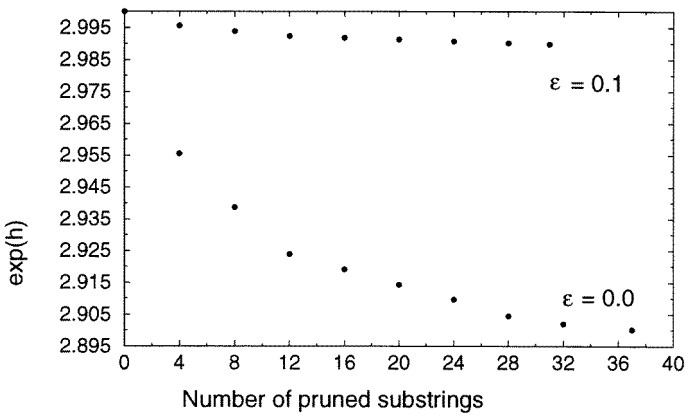

Figure 16. The topological entropy as a function of the number of pruned substrings up to a length of 9 for $\epsilon = 0.1$ and to a length of 8 for $\epsilon = 0$.

immediately gives the information necessary for determining the pruning front.

The stability matrix method, which associates symbols to caustics along trajectories, works well for most trajectories in this system. This method avoids the difficult task of calculating the partition line. The numerical precision of the stability matrix method is slightly below that of the partition line method, but should be sufficient for most applications. We have demonstrated that the methods can be used in zeta-function calculations, and we expect it to be applied in future semiclassical calculations.

Acknowledgments

We want to express our gratitude to Dieter Wintgen who initiated this work. We thank Gregor Tanner, Predrag Cvitanović, Freddy Christiansen and John Briggs for discussions and comments.

References

[1] Friedrich H and Wintgen D 1989 *Phys. Rep.* **183** 37
[2] Hasegawa H, Robnik M and Wunner G 1989 *Prog. Theor. Phys. Suppl.* **98** 198
[3] Delande D 1991 *Chaos in Atomic and Molecular Physics (Les Houches Lectures)* (Amsterdam: North-Holland)
[4] Gutzwiller M C 1990 *Chaos in Classical and Quantum Mechanics* (New York: Springer)
[5] Cvitanović P *et al* Classical and quantum chaos: a cyclist treatise *Preprint* Niels Bohr Institute, Copenhagen (http://www.nbi.dk/∼ronnie/QCcourse).
[6] Tanner G, Hansen K T and Main J 1996 *Nonlinearity* **9** 1641
[7] Smale S 1967 *Bull. Am. Math. Soc.* **73** 747
[8] Bunimovich L A 1995 *Chaos* **5** 349
Bunimovich L A, Sinai Y G and Chernov N I 1990 *Russ. Math. Surv.* **45** 105
Bunimovich L A, Sinai Y G and Chernov N I 1991 *Russ. Math. Surv.* **46** 47
[9] Eckhardt B 1987 *J. Phys. A: Math. Gen.* **20** 5971
[10] Cvitanović P and Eckhardt B 1989 *Phys. Rev. Lett.* **63** 823
[11] Sadovskiĭ D A, Show J A and Delos J B 1995 *Phys. Rev. Lett.* **75** 2120
Main J, Wiebusch G, Welge K, Shaw J and Delos J B 1994 *Phys. Rev.* A **49** 847
Mao J-M and Delos J B 1992 *Phys. Rev.* A **45** 1746
[12] Hansen K T 1992 *Chaos* **2** 71
[13] Hansen K T 1993 *Nonlinearity* **6** 753
[14] Hansen K T 1993 Symbolic dynamics in chaotic systems *PhD Thesis* University of Oslo
[15] Cvitanović P, Gunaratne G H and Procaccia I 1988 *Phys. Rev.* A **38** 1503
[16] Eckhardt B and Wintgen D 1990 *J. Phys. B: At. Mol. Opt. Phys.* **23** 355
[17] Hansen K T 1993 *Nonlinearity* **6** 771
[18] Artuso R, Aurell E and Cvitanović P 1990 *Nonlinearity* **3** 325
Artuso R, Aurell E and Cvitanović P 1990 *Nonlinearity* **3** 361
[19] Abul-Magd A Y and Müller K 1992 *Phys. Rev.* A **46** 7424
[20] Grassberger P and Kantz H 1985 *Phys. Lett.* **113A** 235
[21] Christiansen F and Politi A 1995 *Phys. Rev.* E **51** R3811
Christiansen F and Politi A 1996 *Nonlinearity* **9** 1623
[22] Hansen K T 1995 *Phys. Rev.* E **51** 1838
[23] Eckhardt B and Wintgen D 1991 *J. Phys. A: Math. Gen.* **24** 4335
[24] D'Alessandro G, Grassberger P, Isola S and Politi A 1990 *J. Phys. A: Math. Gen.* **23** 5285
[25] Hansen K T 1992 *Phys. Lett.* A **165** 100
[26] Cvitanović P 1991 *Physica* **51D** 138
[27] Cvitanović P and Eckhardt B 1993 *Nonlinearity* **6** 277